

Spatio-temporal influence of tundra snow properties on Ku-band (17.2 GHz) backscatter

Joshua KING,¹ Richard KELLY,¹ Andrew KASURAK,¹ Claude DUGUAY,¹
Grant GUNN,¹ Nick RUTTER,² Tom WATTS,² Chris DERKSEN³

¹Department of Geography, University of Waterloo, Waterloo, Ontario, Canada

²Department of Geography, Northumbria University, Newcastle upon Tyne, UK

³Climate Research Division, Environment Canada, Toronto, Ontario, Canada

Correspondence: Joshua King <jmking@uwaterloo.ca>

ABSTRACT. During the 2010/11 boreal winter, a distributed set of backscatter measurements was collected using a ground-based Ku-band (17.2 GHz) scatterometer system at 26 open tundra sites. A standard snow-sampling procedure was completed after each scan to evaluate local variability in snow layering, depth, density and water equivalent (SWE) within the scatterometer field of view. The shallow depths and large basal depth hoar encountered presented an opportunity to evaluate backscatter under a set of previously untested conditions. Strong Ku-band response was found with increasing snow depth and snow water equivalent (SWE). In particular, co-polarized vertical backscatter increased by 0.82 dB for every 1 cm increase in SWE ($R^2 = 0.62$). While the result indicated strong potential for Ku-band retrieval of shallow snow properties, it did not characterize the influence of sub-scan variability. An enhanced snow-sampling procedure was introduced to generate detailed characterizations of stratigraphy within the scatterometer field of view using near-infrared photography along the length of a 5 m trench. Changes in snow properties along the trench were used to discuss variations in the collocated backscatter response. A pair of contrasting observation sites was used to highlight uncertainties in backscatter response related to short length scale spatial variability in the observed tundra environment.

KEYWORDS: remote sensing, snow

INTRODUCTION

In the microwave spectrum, changes to the dielectric and physical properties of snow can influence directional scattering components, providing tangible quantities from which to derive information (Ulaby and others, 1984). Given the dynamic nature of terrestrial snow accumulation and metamorphosis, the measured microwave response is not only a function of aggregate snow properties such as snow water equivalent (SWE), but often of stratigraphy and lateral snowpack heterogeneity (Colbeck, 1991). In practical application, the complexities of these interactions are difficult to account for when scales of spatial variability are smaller than the spacing and/or support of the in situ observations used for interpretation. The influence of snow property variability local to an observing instrument can be significant where placement and thickness of dielectric discontinuities can dominate observed backscatter or brightness temperature (e.g. Marshall and others, 2007; Montpetit and others, 2013). Improving understanding of these local-scale interactions specific to distinct snow-cover types is an important step towards the development of robust methods for microwave-based snow property retrieval.

Complex spatio-temporal patterns are common to snow around the world (Deems and others, 2008; Jonas and others, 2009; Scipión and others, 2013), but tundra environments in particular present a challenging target of analysis, with numerous environmental agents acting on shallow depositions of snow on an often rough underlying soil and shrub surface (Derksen and others, 2009; Sturm and Wagner, 2010; Domine and others, 2012). In general, tundra

environments north of the treeline are characterized by low air temperature, exposure to high wind, and little precipitation input (Sturm and others, 1995). Under these conditions, tundra snowpack in open areas forms with contrasting depth-hoar and wind-slab components. Dry snow subjected to strong vertical temperature gradients will undergo metamorphosis, redistributing mass by processes of vapour transport and subsequent grain growth (Sturm and Benson, 1997). Basal layers in tundra environments are often dominated by this process, composed of recrystallized snow microstructure, with grain diameters in excess of 2 mm, and preferential orientation. When sustained winds are present, deposition is quickly redistributed, forming fine-grain (<1 mm) crust and slab features. Over short distances, changes in wind and topography can produce lateral heterogeneity of <1 m up to >100 m (Sturm and Benson, 2004). Electromagnetically, these local variations in bulk and stratigraphic properties have the potential to generate diverse microwave responses from outwardly simplistic targets of similar bulk characteristics (e.g. depth, density, SWE).

A number of purpose-built systems for ground-based radar observation of snow and ice have been introduced in recent years to address questions regarding local-scale interaction (e.g. Marshall and Koh, 2008; Willatt and others, 2010; King and others, 2013; Morrison and Bennett, 2014). These systems have been successfully deployed in support of large field campaigns, including the Cold Land Processes Experiment (CLPX; Marshall and others, 2004), and under-flight testing of proposed satellite missions, such as CoReH₂O (Rott and others, 2010; Chang and others, 2014). Despite recent

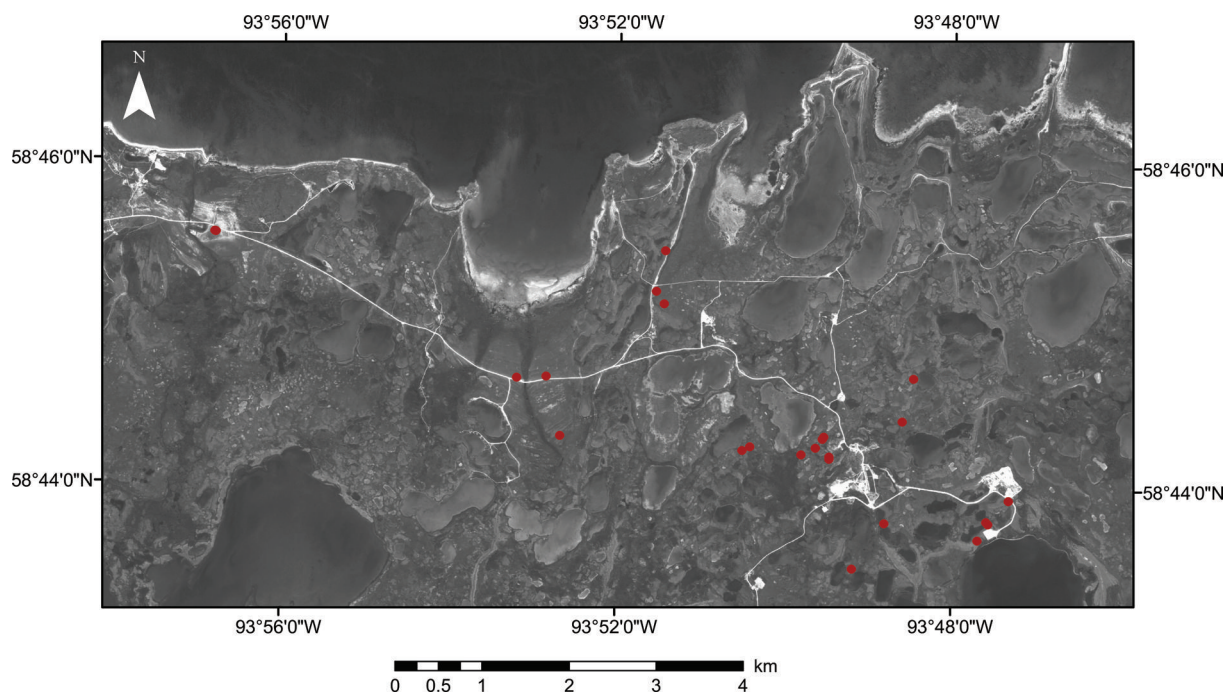


Fig. 1. Churchill study area, with measurement locations indicated in red.

advancements in snow-radar observation, evaluation of the response from snow and substrate in tundra-specific conditions remains incomplete. During the 2010/11 boreal winter, the Canadian Snow and Ice Experiment (CASIX) was initiated to collect coincident backscatter and snow property measurements in a previously unevaluated sub-arctic environment near Churchill, Manitoba, Canada. The field-observed dataset provides a unique opportunity to examine radar sensitivity to snow properties under challenging conditions including shallow depth and prevalent depth hoar.

In this study, we present two destructive sampling procedures to evaluate backscatter against in situ snow properties for the purpose of quantifying and evaluating Ku-band (17.2 GHz) sensitivity in a unique terrestrial tundra environment. As a first case, traditional pit and bulk snow measurements are made within the field of view of an observing radar instrument at a spatially distributed set of snow-covered open tundra sites. Summary and statistical analysis are used to identify and discuss potential drivers of backscatter variability and to quantify Ku-band sensitivity to selected snow properties, including SWE. A second case study presents an enhanced observation protocol using trench excavation and near-infrared (NIR) photography to characterize snow stratigraphy within the radar field of view. Observed heterogeneity of snow properties and stratigraphy are discussed in relation to coincident radar returns measured across the length of the trench. Two sites of contrasting snowpack composition are used to identify potential drivers of backscatter variability and discuss future direction for study. Finally, the observed spatio-temporal backscatter is discussed in the context of previous field studies and electromagnetic models to relate physical contributions to observed backscatter.

STUDY AREA

Churchill (58.7692° N, 94.1692° W) is located on the southwest shore of Hudson Bay at the mouth of the Churchill

River. Proximity to the arctic treeline divides the local environment into a number of distinct tundra/forest transition zones, each with characteristics typical of a larger domain within the circumpolar north (Kershaw and McCulloch, 2007). Access to a number of distinct environments over short distances made Churchill an ideal location to satisfy the diverse observational requirements of CASIX. Measurements collected as part of this study were made in an area to the east of Churchill, primarily composed of open areas (62%) with smaller portions occupied by forest (27%) and lake (11%) features (Derksen and others, 2012). Large expanses of graminoid and shrub tundra were found throughout the study area, with limited vegetation height (<30 cm), little topographic relief (~0–30 m a.s.l.), and underlying organic soils (~5–30 cm in depth) common among them. The prevailing climate conditions in Churchill are best described as sub-arctic, where strong wind ($>5 \text{ m s}^{-1}$), low air temperature ($<-20^\circ\text{C}$) and limited snowfall (201 cm) are defining characteristics of the winter accumulation period.

Backscatter measurements were made between 15 November 2010 and 1 March 2011 at a distributed set of snow-covered open tundra sites along the Hudson Bay coast (Fig. 1). In total, 26 independent radar measurements were completed, along with a suite of coincident snow property measurements to characterize physical processes and variability within the bounds of the observing instrument footprint. By standardizing the observation protocol, a framework for evaluation of inter- and between-site backscatter was established. The mixed land-cover environment local to Churchill provided access to a variety of tundra-class snow conditions, limited in depth by wind exposure and lack of standing vegetation. To minimize environmental and observational complexities, sites were kept free of standing vegetation and anthropogenic modifiers. As such, observations were primarily collected in graminoid-dominated environments where such complexities could be minimized. The following provides a brief overview of the theory and methodology used to characterize the local

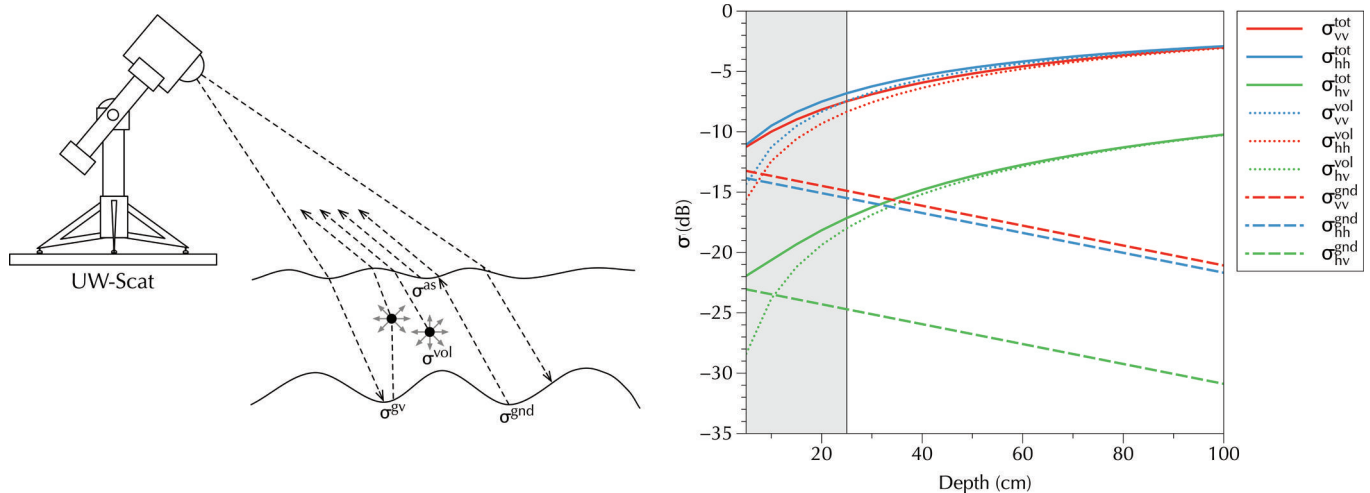


Fig. 2. Left: set-up of UW-Scat, illustrating first-order backscatter for snow-covered terrain (adapted from Rott and others, 2010). Right: composition of theoretical single-layer Ku-band scattering contributions for a snow-covered tundra environment (modelled with the QCA/DMRT implementation of Tsang and others, 2007). Model input parameters: $f = 17.2$ GHz, $\epsilon_{r, \text{gnd}} = 5 + 0.5i$, $\rho = 250$ kg m $^{-3}$, $d = 1$ mm, $\tau = 0.1$ and $\theta = 40^\circ$. Observed range of depth shown in grey.

dynamics of Ku-band radar interaction for the explicit purpose of evaluating sensitivity to tundra snow properties.

DATA AND METHODS

Background

Radar-based snow property retrieval exploits subtle changes in backscatter resulting from variations in accumulation and metamorphosis to derive snowpack information without physical contact. In terrestrial environments, a simple conceptualization of total backscatter (σ^{tot}) can be made with snow- and soil-scattering contributions in a particular transmit-and-receive polarization combination (pq) (Ulaby and others, 1984; Rott and others, 2010):

$$\sigma_{pq}^{\text{tot}} = \sigma_{pq}^{\text{as}} + \sigma_{pq}^{\text{vol}} + \sigma_{pq}^{\text{gv}} + \sigma_{pq}^{\text{gnd}} \quad (1)$$

where the air/snow interface (σ^{as}), snow/ground interface (σ^{gnd}), snow volume (σ^{vol}) and higher-order interactions among the ground and snow volume (σ^{gv}) contribute to total backscatter (Fig. 2). The magnitude of each contribution in Eqn (1) is determined by the dielectric and physical state of the snow-covered environment and the parameters of the observing instrument. With parameters of the observing instrument held constant, spatio-temporal changes in SWE can be expected to exert influence on backscatter because of its inherent relationship with both physical and dielectric properties of the snowpack.

Dielectric properties of target media are commonly described using the complex form of relative permittivity ϵ_r :

$$\epsilon_r = \epsilon' - i\epsilon'' \quad (2)$$

where the real component ϵ' describes the ability of a material to polarize and store energy and the imaginary component ϵ'' is a loss factor describing dissipation of energy, both relative to that of air. For dry snow, values of the imaginary component of permittivity are generally low at microwave frequencies ($\epsilon' < 2$ and $\epsilon'' < 10^{-3}$), resulting in negligible absorption of incident energy, dominant scattering losses, and potential for penetration through meters of snow. If the observed snow becomes wet, the presence of liquid water causes increased reflectivity at the

snow surface ($\epsilon' \approx 20$ – 80), greatly increased attenuation within the snow volume ($\epsilon'' \approx 5$ – 40) and, therefore, diminished potential to retrieve snow properties at microwave frequencies.

Incident energy from a ground-based radar system directed towards a dry snowpack interacts first at the air/snow interface, where it is partially reflected in different directions and partially transmitted into the snowpack. The magnitude of each component depends on the dielectric mismatch between the surface media and air, the roughness at the interface, and the geometry of the radar. In the case of dry snow, the vast majority of incident energy propagates into the volume at incident angles greater than nadir ($\theta > 0$) because of the small difference in permittivity between the air ($\epsilon' \approx 1$) and the snow ($\epsilon' \approx 1.05$ – 2). Assuming a smooth surface, incident energy reflected at the air/snow interface can be estimated using the square of the Fresnel reflection coefficients, where if $\epsilon'_{\text{snow}} = 2$ and $\theta = 40^\circ$, only 5.9% of the horizontally polarized and <1.0% of the vertically polarized incident energy is reflected. As a result, σ^{as} is generally considered to be a minor contributor to dry snow backscatter and is often neglected.

Within the snow volume, variability in σ^{vol} results from changes in physical properties including depth, density and microstructure (Fung, 1994; Tsang and others, 2007; Du and others, 2010). As a mixed medium, dry snow consists of ice crystals in an air background, with ice structures contributing volume scatter at microwave wavelengths. As depth increases, the path length of the propagating wave is extended, increasing the potential for scattering within the volume. A theoretical 17.2 GHz response to increasing depth is demonstrated in Figure 2, where when the quasi-crystalline approximation/dense-media radiative transfer model (QCA/DMRT) of Tsang and others (2007) is parameterized with conditions common to tundra environments, co- and cross-polarized σ^{vol} is found to increase by >10 dB with depths up to 1 m. Open tundra observations in Churchill span a relatively limited range of the demonstrated sensitivity, which coincides with strong increases in σ^{vol} as depth departs from 5 cm. Snow density (ρ) contributes to σ^{vol} through variation in the number of scatterers, and

Table 1. UW-Scat operational parameters

System parameter	Operational value(s)
Height (m)	~2.0
Transmit power (mW)	~10
Centre frequency (GHz)	17.2
Bandwidth (GHz)	0.5
Range resolution (m)	0.3
Beamwidth (°)	4.3
Incident angle (°)	30–45
Footprint at 30° (m)	0.15 × 0.17
Footprint at 45° (m)	0.20 × 0.28
Polarization	VV, VH, HV, HH

consequently the permittivity and the extinction coefficient of the snow volume. A functional relationship exists where $\epsilon' = 1 + 0.0019\rho$, independent of frequency in the microwave spectrum (Hallikainen and others, 1986). According to this relationship, seasonal snow occupies a narrow range of ϵ' between approximately 1.19 and 1.70 (100 and 400 kg m⁻³). Despite the limited range, variation in snow permittivity resulting from seasonal and spatial changes in density can contribute internal reflections and therefore influence σ^{vol} . Higher-order interactions contributing to σ^{vol} are often difficult to quantify, as complexity of the signal is exacerbated by seasonal accumulation and metamorphosis which drive intricate layering, thereby evolving vertical and horizontal heterogeneity of scattering within the snowpack.

The influence of snow metamorphosis on radar response is dictated by a complex set of interactions controlled by grain size, grain shape and aggregate structure. In the case of seasonal snow, processes of vapour transport and subsequent grain growth can exert significant influence on volume scatter as the ratio between grain diameter and wavelength (d/λ) is increased. This relationship is classically defined by Rayleigh scattering theory where scattering is proportional to the fourth power of frequency and the third power of size. In practical application, dependence on grain diameter alone does not account for real-world variations in shape and aggregate structure that may contribute significant portions to observed scatter in addition to multiple scattering between densely packed grains. For example, Du and others (2010) suggest that as the ratio between the long and short axis of a theoretical ellipsoid grain is reduced, cross-polarized response may increase in low to moderate snow volume-scattering environments (i.e. increased depolarization with prolate-shaped grains in shallow snow environments). Similar observations have been made in field studies such as Yueh and others (2009) where a strong seasonal depolarization response was attributed to the development of non-spherical depth-hoar grains. In addition to grain shape, recent studies have suggested that bonding and evolving microstructure can play an important role in observed scatter where aggregate grain structures contribute stronger effective scattering than their individual constituents (Tsang and others, 2007; Chang and others, 2014). Given the potential for dynamic grain growth (0.5 mm $> d < 6$ mm) and development of aggregate depth-hoar structures, it can be expected that metamorphosis of the observed open tundra snowpack will be a notable contributor to the volume-scattering response in addition to bulk properties such as depth or SWE.

If incident microwave energy successfully traverses the snow volume, it is subjected to reflection at the ground surface. Unlike σ^{as} , spatio-temporal variability in σ^{gnd} is common in terrestrial dry snow environments, where local surface properties can exert influence on total backscatter due to the larger dielectric contrast of the surface media ($\epsilon' > 3$) and typically large standard deviation of surface height relative to the wavelength ($h > \lambda/32 \cos \theta$; Ulaby, 1981). Soil moisture and state play an important role in determining reflection where a larger portion of incident energy may be returned into the snow volume when soil is moist and ϵ' is elevated. Seasonally, this is an important consideration when accumulation occurs before the soil has frozen and free moisture is present. Spatially, variation in surface scattering generally results from differences in surface roughness, soil and vegetation type, and heterogeneous soil moisture patterns. In general, σ^{gnd} can be expected to contribute less to total backscatter than σ^{vol} at Ku-band in snow-covered tundra environments (Fig. 2). Energy reflected back into the snowpack may again scatter within the volume and/or scatter within volume followed by reflection from the ground surface, generating higher-order scatter contributions (σ^{8v}).

Backscatter measurement

To characterize backscatter response, a frequency-modulated continuous wave radar system known as the University of Waterloo scatterometer (UW-Scat) was deployed (King and others, 2013). Pulled by snow machine, the Ku-band unit of UW-Scat was transported in a sled-based configuration to terrestrial locations and configured to collect backscatter measurements over a 15 m × 20 m area in <20 min. In the microwave remote sensing of snow, choice of frequency is often a compromise between penetration depth and sensitivity to desired snow properties. At Ku-band (12–18 GHz), the corresponding wavelengths are able to penetrate dry snow to depths >1 m (Mätzler, 1987; Marshall and others, 2004). For the purpose of observing tundra-class snow, Ku-band was therefore sufficient to penetrate the expected range of depths (0.10–0.75 m; Sturm and others, 1995). Moreover, the proximity of the observing instrument wavelength to the scale of individual snow grains was close enough to solicit a large volume response without saturating within the upper bounds of the snowpack. Backscatter measurements made with UW-Scat were collected at a centre frequency of 17.2 GHz across a narrow bandwidth of 0.5 GHz. From the sled-mounted position, the antenna and radio-frequency (RF) hardware operated at a height of ~2.0 m with a narrow beamwidth of 4.3°. The resulting ground-projected radar footprint was <30 cm in azimuth and range directions. Additional operational parameters of use during the experiment are listed in Table 1.

Once an observation site was selected, the scatterometer was levelled to the local terrain and RF hardware was allowed to stabilize at 35°C to minimize temperature effects on the hardware. A two-axis positioning system was then used to direct the radar antenna hardware through a series of azimuth sweeps to collect measurements at elevation angles between 30° and 45° in 3° increments. Measurements at each elevation angle were integrated over a 60° azimuth sweep to improve the number of independent samples and ensure an adequate signal-to-noise ratio. In post-processing, the backscattering coefficient, σ^0 , was estimated to express the ratio of power reflected to power transmitted as

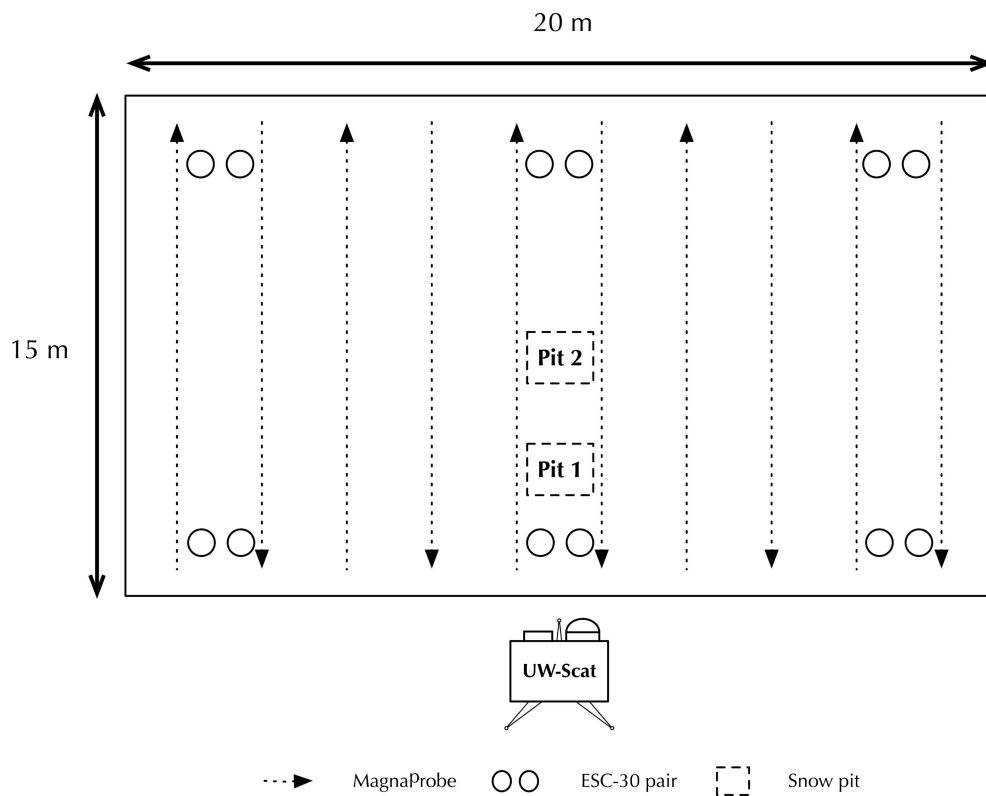


Fig. 3. Destructive snow-sampling protocol plan view. At each site a distributed set of bulk and stratigraphic measurements was made to quantify variability within the scatterometer field of view.

normalized to the ground-projected radar footprint. Co-polarized vertical (σ_{vv}^0), horizontal (σ_{hh}^0) and cross-polarized (σ_{vh}^0) backscatter coefficients were derived based on the averaged range profiles and system geometry. Detailed discussion of signal-processing procedures can be found in Geldsetzer and others (2007) and King and others (2013).

To calibrate the scatterometer system, an accompaniment of internal and external procedures was used. Prior to each site scan, a trihedral corner reflector was erected in the field of view and observed to collect a short time series of measurements. Differences between the observed polarimetric measurements and reference target backscatter were corrected offline using a procedure described by Geldsetzer and others (2007). To characterize system and platform noise, open sky measurements were collected after each corner reflector measurement. Sky measurements were coherently subtracted from target range profiles to reduce the influence of system noise and isolate the desired target signal. Estimates of worst-case measurement error from the post-processing procedure were, on average, ± 2.0 dB including a 0.5 dB addition for random error. In general, the observed errors were a function of the limited number of independent samples collected under the beam-limited conditions of the sled-based configuration as well as bias introduced by human and environmental inaccuracies with misestimation of the deployed sensor height and wind buffing of the reference target. A detailed discussion of the error estimation process can be found in King and others (2013).

Snow measurements

Destructive sampling within the scatterometer field of view was completed immediately after each scan to gather information about local snow properties and to evaluate

snow variability at the sub-scan level. A standard procedure was used where horizontal heterogeneity in depth, density and SWE was quantified in addition to point measurements of vertical snow properties. On completion of the scatterometer measurement, a 15 m \times 20 m box was measured within the field of view of the scatterometer to bound a snow-sampling area (Fig. 3). Within the sampling area, a grid of snow depth measurements was collected using a GPS-enabled Snow-Hydro MagnaProbe. Each grid contained a minimum of 200 measurements spaced across several transects parallel to the scatterometer range direction. Pairs of snow-core measurements were also collected at six locations within the sampling area to estimate bulk density and SWE. The snow-coring instrument had a cross section of 30 cm² and is often referred to in the literature as the ESC-30 (Pomeroy and others, 1997; Derksen and others, 2012; Rees and others, 2014). Using a handheld spring scale, the weight of each snow core was recorded, along with the depth at the measurement site.

In addition to bulk snow measurements, two snow pits were excavated at 3 and 5 m outwards from the scatterometer using standardized procedures (Fierz and others, 2009). Multiple snow pits were completed to avoid mischaracterization related to pit placement and large variations in topography (e.g. hollows between hummocks). Once excavated, structural and textural discontinuities were used to define and record layer locations, thickness and general composition. A snow sample from each layer was extracted and placed on a grid comparator card for visual analysis. Using a stereo-microscope, grain origin types were identified and estimates of axial diameter were recorded. Density within each snow pit was measured along two continuous vertical profiles extracted from the pit face using

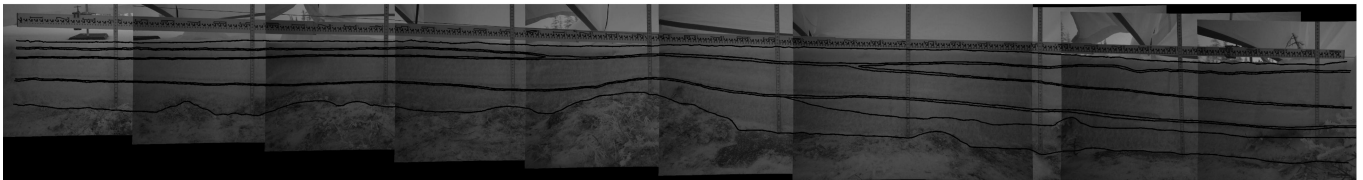


Fig. 4. A series of 850 nm NIR photographs taken along the length of an excavated 5 m snow trench. Photographs were referenced and stitched together for analysis. Black lines show manually identified snow stratigraphy.

a 100 cm³ box-style cutter and digital scale. Temperature profiles were constructed using a string of thermistors inserted into the snowpack with a vertical spacing interval of 4 cm.

Trench measurements

To evaluate the influence of lateral heterogeneity on backscatter, detailed measurements of snowpack stratigraphy were excavated within the scatterometer field of view. Following a protocol detailed by Tape and others (2010), a 5 m trench was dug ~3 m outwards from the scatterometer across the azimuth look direction to correspond with scatterometer measurements collected at elevations between 30° and 45°. The excavated face was prepared manually with hand tools to create a flat surface perpendicular to the ground surface. Once prepared, 850 nm centre frequency NIR photography was completed along the length of the trench using a linear rail system to maintain a

constant distance to the trench face. Sequential photographs taken along the length of the trench were georeferenced using an in-scene cm-scale measuring staff positioned horizontally above the trench face. A single continuous image was stitched together from the collected set of photographs, and stratigraphy was manually extracted at a 1 cm horizontal resolution (Fig. 4). In addition to NIR photography, inter-layer snow properties were characterized with a set of five snow pits completed at 1 m intervals along the trench. Vertical transects of density, temperature and grain size were measured using the previously described standard snow-pit protocol.

RESULTS

Seasonal and spatial snow properties

Accumulation within the Churchill study area evolved with spatio-temporal complexity related to variations in vegetation, topography and climate. Given the selected land-cover composition of flat open terrain and dominant graminoid vegetation, observation sites were exposed to a common set of sub-arctic environmental agents including strong wind and sustained low air temperature. The majority of accumulation within the study area was deposited between December and January, with a limited number of precipitation events occurring thereafter. In the observed open areas, snowpack development was heavily influenced by sustained winds, where average speeds commonly exceeded 5 m s⁻¹, rapidly redistributing accumulated snow. Mean snow depth at the observed tundra sites was shallow, ranging from approximately 4 to 25 cm, generally increasing through the season (Table 2). Examples at the extreme of this range were associated with changing land-cover characteristics found in close proximity to the observation site (e.g. forest transition zones situated near sites 14 and 15). Inter-site standard deviation of snow depth ranged between 20% and 64% of the mean, in most cases declining with increasing depth ($R = -0.5$, $n = 26$; correlations and coefficients of determination were significant at the 0.05 level). At the open tundra sites, microtopographic elements, including hollows between hummocks, trapped early-season snow and created deviations by up to double the inter-site mean. The influence of these features on total depth was reduced as accumulation increased relative to variations in surface height, effectively masking the smaller ground features. Despite the sustained influence of wind, bulk snow density remained low (<250 kg m⁻³) and did not vary substantially through the season. Compared to depth, inter-site variability of density was smaller at a majority of sites, with standard deviations accounting for 9–46% of the mean. As a product of depth and density, the observed range of SWE was seasonally and spatially limited to 70.0 mm or less. At the tundra observation sites, variation in SWE showed a stronger linear relationship

Table 2. Inter-site snow properties measured at each tundra observation site. Dates of observation are presented as day of year (DOY) spanning the 2010/11 observation period. Bulk SWE and density measurements were not available on DOY 60

Site	DOY	Depth		Density		SWE
		Mean cm	SD cm	Mean kg m ⁻³	SD kg m ⁻³	Mean mm
1	310	5.7	2.9	104	10	5.9
2	319	5.0	2.9	139	40	6.9
3	320	5.3	1.8	129	51	6.9
4	320	3.9	1.0	154	54	6.0
5	322	3.5	1.3	139	40	4.8
6	324	4.0	1.5	155	71	6.3
7	328	6.2	2.7	258	70	15.9
8	328	6.9	2.8	262	41	18.1
9	329	3.9	1.4	112	26	4.3
10	329	4.1	1.4	130	31	5.3
11	334	8.1	1.9	206	41	16.7
12	337	11.6	3.7	288	91	33.3
13	337	10.9	4.6	211	32	22.9
14	346	23.2	6.7	302	40	70.0
15	346	24.1	6.6	207	29	49.9
16	352	14.0	3.6	186	22	26.0
17	4	16.2	4.3	253	30	41.0
18	16	20.5	13.2	163	41	33.3
19	17	14.0	3.6	219	33	30.8
20	24	16.9	4.6	264	43	44.6
21	33	19.0	6.0	248	42	47.0
22	44	16.8	6.0	280	34	46.9
23	49	19.2	7.2	233	36	44.6
24	50	21.9	6.0	216	34	47.2
25	56	15.2	4.3	209	29	31.8
26	60	25.0	5.0	–	–	–

with depth ($R^2 = 0.98$) than density ($R^2 = 0.46$) as a result of the smaller range of bulk density encountered.

Snow stratigraphy excavated within the scatterometer field of view increased in complexity from an early point in the experiment. Sequential periods of accumulation and wind transport created two to seven distinct horizontal layers of varied thickness and texture. A basal depth-hoar layer was the most consistent feature excavated among the open tundra sites. In the 50 pits completed, depth hoar comprised, on average, 52% of total depth. The rapid development of the basal hoar layer was driven by a sharp early-season decline in air temperature sustained through the end of the experiment with limited increases in depth. Vertical temperature gradients measured through the shallow snowpack exceeded 20°C m^{-1} in 40 of 50 open tundra pits, a strong indicator of sustained kinetic growth. Well-defined cups were a common feature of the basal depth-hoar layer, with large aggregations present from DOY 334 onward. By the end of the observation period, grains within the depth-hoar layer had exceeded 3 mm in major axis diameter, with poly-aggregates reaching 6 mm or larger (Fig. 5). Thickness of the basal depth-hoar layer was heavily influenced by inter-site changes in ground surface height. As a result, the thickness of the basal hoar layer between inter-site snow pits was found to vary by up to 10 cm where periodic hummock features were present.

Contrasting snow surface features were heavily influenced by wind transport, featuring multiple slab layers separated by hard thin crusts. Grain diameter within the surface slab layers was generally small (<1 mm) due to persistent wind action and subsequent rounding of grains with transport. A vertical gradient of grain diameter became apparent in the latter part of the experiment, where wind-rounded grains transitioned into solid facets with sustained temperature gradient metamorphosis. In several of the late-season snow pits, large faceted grains were found inter-mixed all the way to the surface of the snowpack. Few ice features were identified, with those found being very thin snow-ice layers situated at the base of the pack from early-season melt processes. Rapid redistribution of snow accumulation limited the number of fresh-snow observations collected during the experiment; in most cases, surface layers identified with fresh snow were <2 cm thick and intermixed with wind-rounded grains.

Overall, the rapid and often subtle changes within the shallow tundra snowpack provided a challenging target of analysis and a unique opportunity to evaluate distinctive features previously unaddressed at Ku-band. The predominant local processes of wind redistribution and temperature gradient metamorphosis were characteristic of conditions previously described along the Hudson Bay coast and of general conditions present with tundra-type snow (Sturm and others, 1995; Kershaw and McCulloch, 2007; King and others, 2013). Electromagnetically, the early and rapid development of large depth hoar had the potential to drive strong increases in backscatter as seasonal and spatial processes of accumulation and metamorphosis progressed.

Comparison of backscatter measurements and snow properties

To evaluate spatio-temporal backscatter sensitivity, snow property measurements collected at each site were compared against coincident estimates of σ^0 . In an effort to reduce the influence of sub-scan variations in

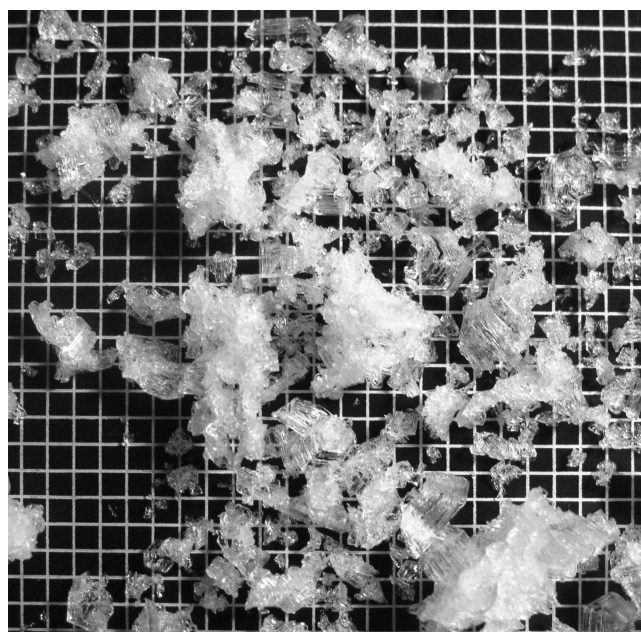


Fig. 5. Basal depth hoar at site 25 on a 2 mm grid comparator card. The large aggregations found at site 25 were common to most observation sites from DOY 334 forward.

microtopography, estimates of σ^0 were averaged to integrate a number of azimuth sweeps across a small range of incident angles between 30° and 45° . In the averaged scatterometer measurements, the dynamic range of σ^0 was found to be >8 dB. Co-polarized σ_{vv}^0 and σ_{hh}^0 ranged in magnitude from approximately -13 to -5 dB while cross-polarized σ_{vh}^0 and σ_{hv}^0 responses were measured across a lower and smaller range between -26 and -15 dB. For the entirety of the experiment period, cross-polarized σ_{vh}^0 and σ_{hv}^0 were found within 0.1 dB and therefore were considered reciprocal for the purpose of analysis.

The observed relationships between depth, SWE and σ^0 , as shown in Figure 6, indicate Ku-band sensitivity to evolving snow properties at the 26 open tundra sites. Across the small range of encountered depth, a clear linear relationship with σ_{vv}^0 emerged, where vertically polarized backscatter increased by ~ 0.22 dB for every 1 cm increase in depth ($R^2 = 0.67$). A slightly less sensitive σ_{hh}^0 response, not shown in Figure 6, increased by 0.17 dB for every 1 cm in depth ($R^2 = 0.44$). The observed sensitivity agrees with the theoretical relationship demonstrated in Figure 2, where increasing path length generates a strong volume response in shallow snow with large grains (>1 mm). Preferential vertical scattering was apparent throughout the experiment, where 18 of 26 observations demonstrated a co-polarization ratio ($\sigma_{hh}^0/\sigma_{vv}^0$) less than 0. The Ku-band co-polarization ratios were moderately correlated with the number of layers observed within the scatterometer field of view ($R = -0.64$) suggesting that rough surface interactions within the layered accumulation played a role in the observed horizontal response. Alternatively, it is possible that the observed vertical arrangement of depth-hoar aggregates along the path of vapour transport contributed to the stronger vertical response. The cross-polarized σ_{vh}^0 response was comparable in slope to the co-polarized, increasing by ~ 0.17 dB for every 1 cm increase in depth ($R^2 = 0.39$). The coevolution

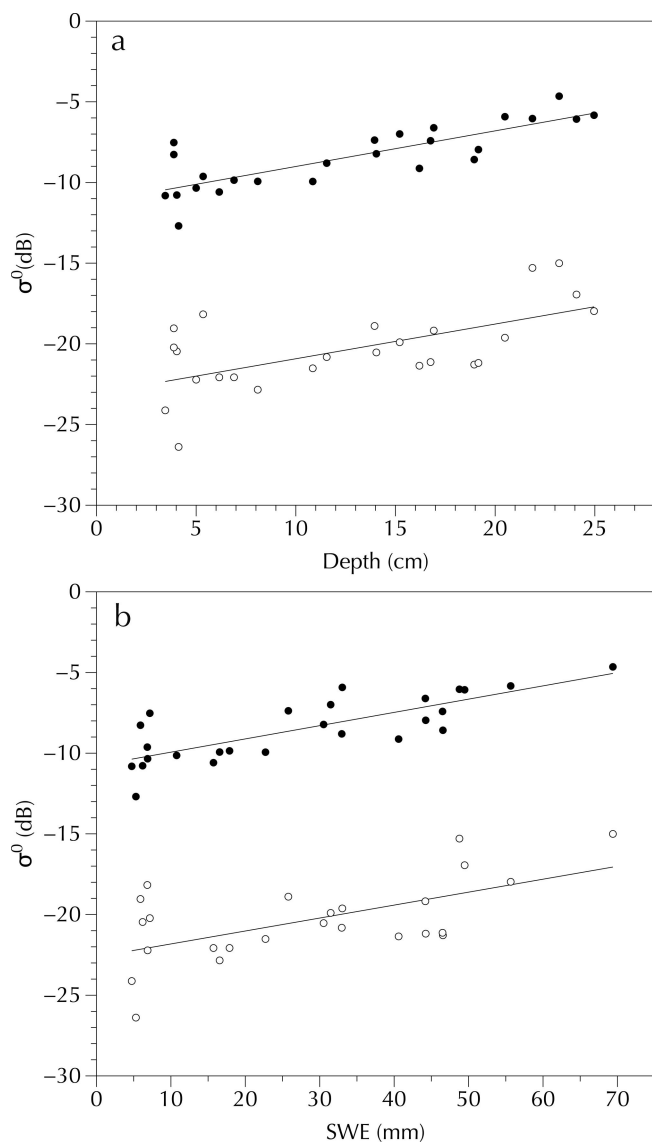


Fig. 6. Comparison of σ^0 averaged for incident angles between 30° and 45° against snow depth (a) and SWE (b) at each tundra observation site. Solid circles show σ_{vv}^0 response, and hollow circles show σ_{vh}^0 response. Measured σ_{hh}^0 and σ_{hv}^0 responses not shown, to improve readability.

of the co- and cross-polarized response was reflected in a small standard deviation of the depolarization ratio ($\sigma_{vh}^0/\sigma_{vv}^0$), where σ_{vh}^0 was generally 9–14 dB lower than σ_{vv}^0 . The strong cross-polarized backscatter is indicative of multiple scattering between density-packed grains and/or the presence of non-spherical snow grains (Tsang and others, 2007; Yueh and others, 2009; Du and others, 2010).

Similar to snow depth, spatio-temporal variation in SWE was limited by persistent wind action and negligible precipitation input. Despite this, the observed increase in σ^0 was large relative to the small range of observed SWE. Sensitivity to SWE was strongest with σ_{vv}^0 , increasing by 0.82 dB for every 1 cm in SWE ($R^2 = 0.62$). Similar to the observed relationship with depth, σ_{hh}^0 showed a lower but significant sensitivity to SWE at 0.62 dB for every 1 cm increase ($R^2 = 0.42$). Finally, the cross-polarized σ_{vh}^0 sensitivity was observed at 0.80 dB for every 1 cm increase in SWE ($R^2 = 0.36$). In the relationship between SWE and σ^0 ,

backscatter diversity often separated sites of similar aggregate composition, in some instances by several decibels. This finding highlights the complexity of the observed interaction space, where density, grain size and vegetation/soil properties are important contributors to backscatter in addition to variation in depth. Seasonality and metamorphic state of the snowpack appeared to play a role in the observed backscatter diversity where increases in the major axis diameter of grains measured with a grid comparator card were moderately correlated with increased vertical backscatter ($R = 0.39$). The identified relationship with grain diameter was not found to be significant with horizontal or cross-polarized backscatter. While this finding is of interest, the seasonality of the measurements and, as a result, covariance of depth and grain growth made it difficult to decompose causation between the evolving snow properties. Moreover, the previously demonstrated spatial variability in stratigraphy made it extremely difficult to interpret the inter-site snow pits in the context of the larger scatterometer field of view. Overall, the distributed measurement protocol was able to identify Ku-band sensitivity to bulk snow properties when both in situ measurements and radar observations were averaged up to the site scale, but did not provide the means to quantify the role of stratigraphy, grain size and surface properties in observed backscatter diversity.

Evaluation of trench backscatter response

Direct comparison of in situ sampled snow properties and σ^0 revealed Ku-band sensitivity to increasing snow volume. Despite the positive result, snow pits completed within the scatterometer field of view yielded insufficient information to evaluate the influence of sub-scan lateral heterogeneity on observed backscatter. To address this open question, two 5 m trench experiments were completed on 7 and 8 January to characterize variation in stratigraphy within the scatterometer field of view. Collocated radar returns measured across the azimuth range of the scatterometer were compared with excavated snow stratigraphy to evaluate potential sub-scan influences on backscatter. The first trench was excavated in an open area adjacent to a transition zone, hereafter referred to as the forest edge site. The forest edge site possessed snow features common to the previous open tundra sites including limited depth, predominant wind-slab/depth-hoar composition and a rough underlying ground surface. The second trench was completed within a sparsely populated tree stand where the sheltered snowpack was composed of a larger number of lower-density layers. Comparison of the two targets provided an opportunity to evaluate a range of snow conditions and their influence on backscatter at scales local to the observing instrument.

A complex arrangement of internal layers with several discontinuous features was observed at the forest edge site (Fig. 7a). Within the shallow snowpack, three to five distinct layers were found at any given horizontal position, and, in total, six unique layers were identified. Total snow depth along the trench varied between 16.4 and 37.2 cm with a standard deviation of 5.6 cm (Fig. 7b). The observed variation in depth was in agreement with inter-site measurements completed at the previous open tundra sites, where large changes in total depth were encountered over short distances. The most prominent change in snowpack composition was associated with a protruding hummock feature centred at the midpoint along the trench. Prior to excavation, the smooth surface of the mid-season snowpack

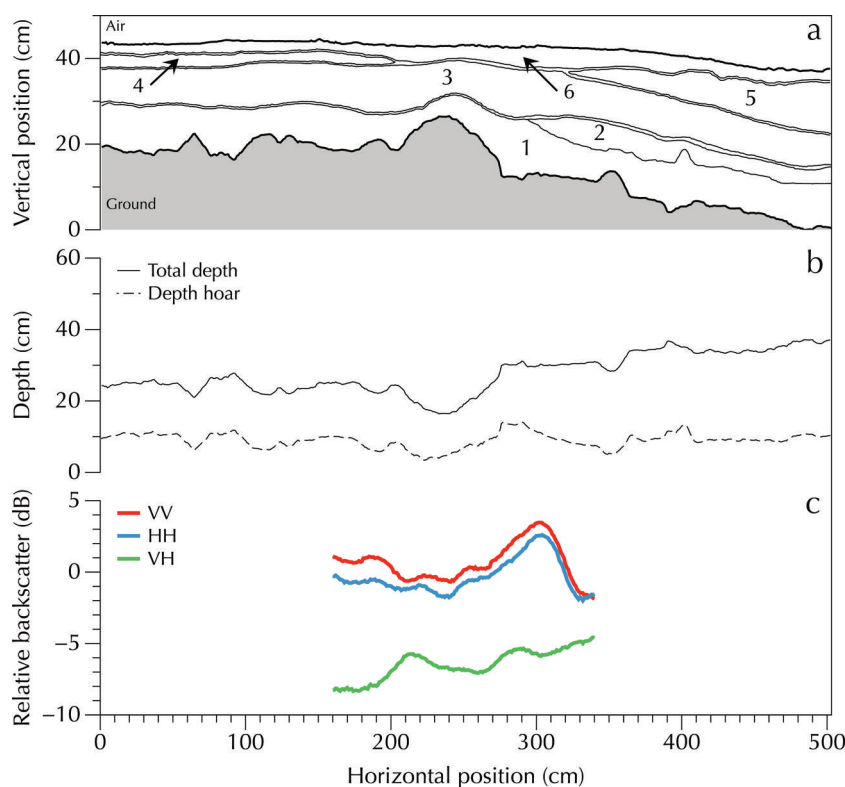


Fig. 7. Stratigraphy (a), depth (b) and relative backscatter (c) observed along the length of the forest edge trench. Layer notation in (a) corresponds to description in Table 3.

provided no indication of the heavy influence of this feature on both total depth and stratigraphy.

Internal stratigraphy of the forest edge snowpack consisted of several wind-influenced features underlain with a continuous layer of depth hoar (Table 3). A number of thin wind crusts (<0.5 cm), harder in texture than the surrounding snow, separated the larger internal layers of the snowpack. The upper and most recent feature, noted as layer 6 in Figure 7, was a smooth continuous surface layer composed of small wind-rounded grains intermixed with decomposing needle-like precipitation (0.1–0.4 mm). Beneath layer 6, a set of thin soft slabs, noted as layers 4 and 5, surrounded the apex of the prominent hummock feature where wind scouring had created a notable horizontal discontinuity. Each slab was composed of slightly larger wind-rounded grains (0.4–1.0 mm) and was similar in density to the surface slab layer (220 kg m^{-3}). The largest continuous feature identified within the trench was a mixed-type layer composed primarily of faceted grains identified as layer 3. Within this large continuous layer, a wide range of grain size was found (0.2–1.5 mm). On the right-hand side of the trench, a hard relict wind slab was identified as layer 2 (3–5 m) in which densities were the highest within the snowpack, increasing to $\sim 280 \text{ kg m}^{-3}$. The basal surface of layer 5 was composed of high-density indurated hoar with well-developed cup structures >1 mm in diameter. Finally, the basal depth-hoar layer, noted as layer 1, contained striated cup-shaped grains and large poly-aggregates ranging in diameter from 1 to 4 mm. As a fraction of total depth, the depth-hoar layer composed on average 33% or 9.0 cm of the snowpack (Fig. 8b). The thickness of the basal layer was controlled by the ground surface height and location of the buried hard slab.

The excavated trench revealed an interesting target for radar observation where large changes in snowpack properties were found over short distances. Radar measurements collected as part of the forest edge scan were processed as individual returns relative to response of the collocated corner reflector and given approximate horizontal positions in relation to the trench face (Fig. 7c). As a general limitation of the observation protocol, uncertainty in the estimated horizontal radar position was greatest near the edges of the scan due to the arc of ground projected scatterometer sweep. The measured co-polarization response across the trench showed variability in relation to changing snow and soil conditions. In particular, variability

Table 3. Description of stratigraphy excavated at the forest edge site. Layer numbers correspond to Figure 7

Layer	ICSSG* code	Description
6	RGwp (DFbk)	Recent mixed layer with wind-rounded grains and decomposing needles
5	RGwp (FCsf)	Mixed soft slab layer composed of mostly wind-rounded grains
4	RGwp (FCsf)	Mixed soft slab layer composed of mostly wind-rounded grains
3	RGwp (FCsf)	Mixed soft slab layer with wind-rounded and faceted grains
2	FCso (RGxf)	Buried hard slab. Mixed composition of indurated hoar
1	DHch	Depth hoar. Large faceted cups and poly-aggregate structures

*International Classification for Seasonal Snow on the Ground.

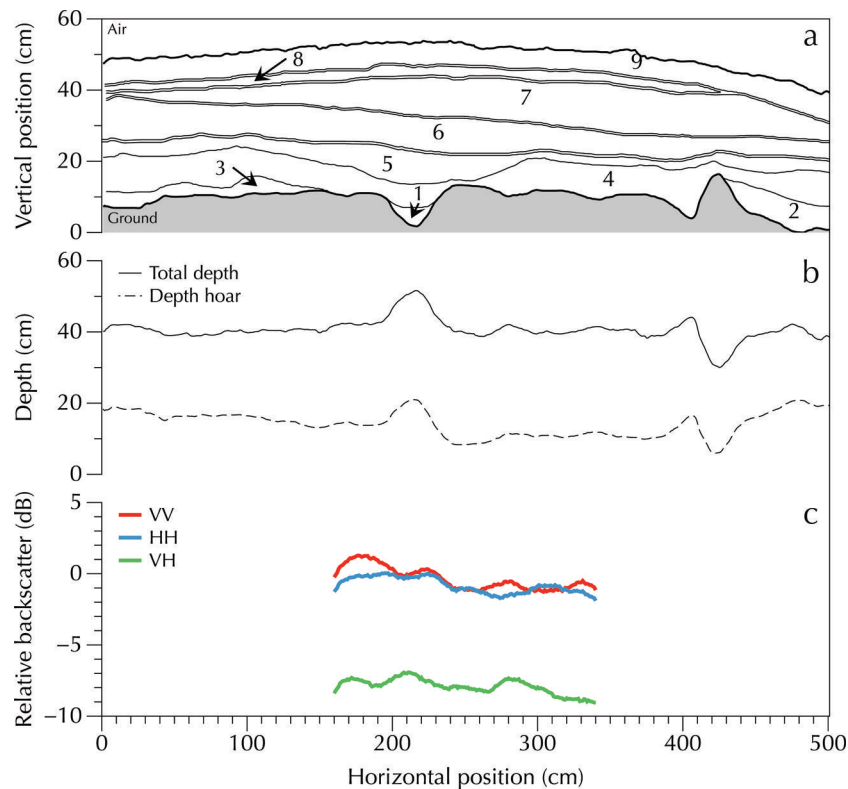


Fig. 8. Stratigraphy (a), depth (b) and relative backscatter (c) observed along the length of the forest trench. Layer notation in (a) corresponds to description in Table 4.

was noted in relation to the previously identified hummock feature where co-polarized vertical backscatter decreased by 16% relative to the deeper accumulation situated at horizontal positions to the left of the feature. The horizontal backscatter response to the large change in snow depth was muted in comparison, emulating previously observed behaviour of the low co-polarization ratio observed in the distributed set of tundra snow targets. Across the width of the trench, co-polarized horizontal response was found to be ~12% lower than the vertical response. To the right of the hummock, backscatter increased, reaching a trench maximum near the horizontal position of 3 m. The rapid increase in co-polarized backscatter coincided with

increasing snow depth and complexity in layering. In particular, layer 5 was a unique dielectric and geometric discontinuity where the indurated depth hoar was both of higher density and larger grain size compared to the surrounding layers. Coupled with the increased depth to the right of the hummock, there was potential for multiple scattering, which appeared to be supported by the increased depolarization. Overall, the forest edge trench demonstrated the presence of dynamic changes in snowpack structure over short distances, which appear to have had a large influence on backscattered energy.

The second trench was completed within a sparsely populated tree stand, sheltered from strong local winds. Total depth along the trench ranged from 30.0 to 51.6 cm, with a smaller standard deviation of 3.1 cm. The contrasting influence of the local environmental agents was evident in the excavated stratigraphy (Fig. 8). Here layers were comparatively homogeneous, greater in number and, in most cases, found continuously through the 5 m trench. In total, nine unique layers were identified, with five present across the entire trench (Table 4). As in the previous excavation, a number of thin crusts (<1 mm) were found separating the major internal layers. Fresh precipitation, identified as layer 9, was the most recent layer and was composed of a combination of large stellar plates (1 mm) and much smaller graupel (0.1 mm). Below the fresh snow surface, a decomposing precipitation layer was found with smaller round grains (layer 8). Lacking influence from local wind, the two most recent layers were very low in density, ranging from approximately 100 to 150 kg m⁻³. The remaining layers of the snowpack were heavily influenced by temperature gradient metamorphosis, with grain size increasing towards the base of the snowpack. Layer 7, the more recent of two mixed-type layers, was composed of

Table 4. Description of stratigraphy observed along the length of the forest trench. Layer numbers correspond to Figure 8a

Layer	Code	Description
9	PPsd (PPgp)	Fresh snow. Stellar plates and graupel present
8	DFdc (RGlR)	Recent snow. Decomposing precipitation and clusters of rounded grains
7	FCso	Mixed layer. Primarily composed of small rounded grains with some faceted grains present
6	FCso	Mixed layer. Primarily composed of larger loose faceted grains with some round grains
5	DHcp	Unconsolidated depth hoar. Mix of cups and less developed forms
4	DHcp	Unconsolidated depth hoar. Large cup-shaped grains
3	DHch	Consolidated depth hoar. Hard texture
2	IFbi	Icy layer. High-density hard-snow feature
1	IFbi	Icy layer. High-density extremely hard-snow feature

smaller rounded grains with some larger faceted grains (0.3–1.0 mm). A similar mix of grain types was found in layer 6, with a bias towards larger faceted grains (0.6–1.8 mm). Density increased within the more mixed layers, reaching a maximum of 270 kg m^{-3} . Again, basal depth-hoar features dominated the remainder of the snowpack, with layers 4 and 5 composed of large cup-shaped grains up to 4 mm in diameter. Density within the unconsolidated depth-hoar layers was lower, at $\sim 170 \text{ kg m}^{-3}$. A number of discontinuous icy hoar features, identified as layers 1, 2 and 3, were found at the base of the pack. These thin features were very hard in texture and were composed of large grains up to 4 mm in diameter.

Compared to the forest edge trench, the backscatter response from the forest trench was stable across the scan. The reduced variability in the co- and cross-polarized backscatter corresponded well to reduced variation in snow depth and increased homogeneity of the internal stratigraphy relative to the previous trench. In clear contrast to the forest edge site, there was no observed preference in orientation of the co-polarized backscatter. This observation separates the forest response from the open tundra sites where vertical preferential scattering was consistently observed. Across the full length of the trench, a decline was identified in both the co- and cross-polarization response. This observed variation in backscatter was small compared to the previous trench, but did indicate a changing interaction with the physical and/or dielectric properties of the sub-scan target. The most evident change in snowpack composition along the trench that could have produced an attributable change in backscatter was the increasing thickness of layer 7 and corresponding reduction of layer 6. These two mixed-layer types were composed of different grain sizes, those within the more recent layer 7 being significantly smaller in diameter. From left to right, layer 7 gradually became the dominant snowpack layer, effectively reducing the mean grain size of the snowpack. Unfortunately, the coarse range resolution of UW-Scat did not allow for characterization of individual layer contributions, and so did not offer definitive evidence of why the change had occurred.

In general, the contrasting backscatter responses of the two trench sites provided practical examples of the influence of sub-scan snow properties on Ku-band backscatter. The findings suggest that variability in tundra snow and soil properties over short distances are significant modifiers of Ku-band backscatter and, in the future, should be considered in the development of tundra snow property retrievals. When in situ and radar measurements were averaged up to the trench (5 m) scale, there was clear sensitivity of backscatter to SWE. Comparisons at smaller scales likely require high-resolution radar systems to separate contributions to backscatter as a function of depth and horizontal location.

DISCUSSION AND CONCLUSIONS

During CASIX, a distributed set of 26 backscatter measurements were collected across a range of tundra snow conditions influenced by spatio-temporal processes of accumulation and metamorphosis. A standardized sampling protocol was introduced to measure snow properties within the scatterometer field of view immediately after each scan to evaluate local influences on backscatter. Predominant agents of wind transport and temperature gradient

metamorphosis governed the spatio-temporal development of the observed snowpack at the selected open tundra sites. Sustained exposure to strong winds quickly redistributed accumulation, and combined with the dry polar environment, limited total depth to typically <30 cm. Inter-site variations in snow depth were often large as a result of changes in underlying ground surface and vegetation height that varied over short distances. Given the anticipated sensitivity of Ku-band to changing snow conditions, the inter-site variations in depth had the potential to drive variability in sub-scan backscatter measurements. In addition to wind action, steep vertical temperature gradients were common to the open tundra sites, which enabled periods of substantial grain growth. A thick basal depth-hoar layer was found throughout the experiment, with large cup-shaped grains with diameters in excess of 4 mm. By the end of the observation period, faceted grains were found throughout the full volume of the snowpack, with large aggregations present in the basal layers.

Despite limited accumulation, a large dynamic range of co- and cross-polarized σ^0 was observed at the open tundra sites. Analysis of the spatio-temporal response indicated Ku-band backscatter sensitivity to increasing snow depth and SWE. This finding is in agreement with previous airborne measurements made by Yueh and others (2009), where strong co- and cross-polarized Ku-band (13.4 GHz) responses were observed at a number of CLPX-II terrestrial sites in Colorado (0.5 dB for every 1 cm SWE). In general, the Churchill response to SWE appears to have been stronger but shows similarity to the shallow snow observations at the CLPX-II North Park site (0.15–0.5 dB for every 1 cm SWE). Here steep temperature gradients through the shallow snowpack (<37 cm) at both sites provided the conditions necessary for the development of depth hoar, and, as a result, strong snow volume responses over a relatively limited range of SWE. The development of large and/or clustered depth-hoar grains such as those shown in Figure 5 had the potential to enhance the radar response with strong forward scattering and increased multiple scattering within the snow volume (Marshall and others, 2004; Du and others, 2010). Recent advancement in DMRT theory supports this finding, where clustering of grains, described as stickiness (τ), has been shown to generate strong scattering effects comparable to grains of a much larger effective diameter (e.g. Tsang and others, 2007; Chang and others, 2014). Prominent aggregations clustered along paths of vertical vapour transport within the Churchill snowpack are a likely contributor to the enhanced backscatter response and will be a subject of future study.

While the distributed open tundra scatterometer observations showed sensitivity to evolving snow properties, in agreement with previous field and model observations, inter-site measurements were insufficient to characterize the influence of sub-scan variations in snow properties. With demonstrated variability in depth and stratigraphy over short distances, a refined methodology for detailed characterization of snow stratigraphy within the field of view was implemented. Two detailed trench experiments, completed in contrasting environments, exemplified the highly variable nature of tundra snow despite its shallow accumulation. The influence of variability in snow properties was apparent in the backscatter signal at the forest edge site where deviations of depth and stratigraphy created strong deviations in signal. Conversely, the relative homogeneity of the forest trench site

responded with reduced variability in backscatter. In the future, snow property information extracted from trench experiments will be of use to initialize electromagnetic models and for diagnostic analysis where sensitivity of high-resolution snow properties can be evaluated over the entire trench. Such studies will be particularly useful for clarifying the role of grain size where subtle changes in layer structure have appeared to influence backscatter.

This study has presented a novel set of ground-based experiments to evaluate the influence of spatio-temporal changes in snow properties on Ku-band backscatter. In doing so, a previously untested sub-arctic tundra environment has been characterized, providing a starting point for the development of robust retrieval methods. The findings of this study support the use of Ku-band backscatter measurements for observation of snow properties in tundra environments. Future study will be needed to assess the implications of the demonstrated backscatter variability with snow accumulation and its influence on scaling to airborne and satellite-based observation approaches.

ACKNOWLEDGEMENTS

CASIX field activities were supported by the European Space Agency, Environment Canada and the Natural Sciences and Engineering Research Council of Canada (NSERC). We thank Arvids Silis, Cristina Surdu, Dave Halpin, Homa Kheyrollahpour, Jason Oldham, Mel Sandells, Nic Svacina, Niina Luus, Peter Toose, Ryan Ahola and Steve Howell for their contributions to the field campaign. Logistical support for CASIX was provided by the Churchill Northern Studies Centre. The University of Waterloo scatterometer system was developed with support from the Canadian Foundation for Innovation and the Ontario Ministry of Research and Innovation. The work of Joshua King, Richard Kelly, Grant Gunn and Claude Duguay was supported by the NSERC. We thank two anonymous reviewers who greatly improved the quality of the paper.

REFERENCES

- Chang W, Tan S, Lemmetyinen J, Tsang L, Xu X and Yueh SH (2014) Dense media radiative transfer applied to SnowScat and SnowSAR. *IEEE J. Select. Topics Appl. Earth Obs. Remote Sens.*, **7**(9) (doi: 10.1109/JSTARS.2014.2343519)
- Colbeck SC (1991) The layered character of snow covers. *Rev. Geophys.*, **29**(1), 81–96 (doi: 10.1029/90RG02351)
- Deems JS, Fassnacht SR and Elder KJ (2008) Interannual consistency in fractal snow depth patterns at two Colorado mountain sites. *J. Hydromet.*, **9**(5), 977–988 (doi: 10.1175/2008JHM901.1)
- Derksen C and 6 others (2009) Northwest territories and Nunavut snow characteristics from a subarctic traverse: implications for passive microwave remote sensing. *J. Hydromet.*, **10**(2), 448–463 (doi: 10.1175/2008JHM1074.1)
- Derksen C and 6 others (2012) Evaluation of passive microwave brightness temperature simulations and snow water equivalent retrievals through a winter season. *Remote Sens. Environ.*, **117**, 236–248 (doi: 10.1016/j.rse.2011.09.021)
- Domine F, Gallet J-C, Bock J and Morin S (2012) Structure, specific surface area and thermal conductivity of the snowpack around Barrow, Alaska. *J. Geophys. Res.*, **117**(D14), D00R14 (doi: 10.1029/2011JD016647)
- Du J, Shi J and Rott H (2010) Comparison between a multi-scattering and multi-layer snow scattering model and its parameterized snow backscattering model. *Remote Sens. Environ.*, **114**(5), 1089–1098 (doi: 10.1016/j.rse.2009.12.020)
- Fierz C and 8 others. (2009) *The international classification for seasonal snow on the ground*. (IHP Technical Documents in Hydrology 83) UNESCO–International Hydrological Programme, Paris
- Fung AK (1994) *Microwave scattering and emission models and their applications*. Artech House, Norwood, MA
- Geldsetzer T, Mead JB, Yackel JJ, Scharien RK and Howell SEL (2007) Surface-based polarimetric C-band scatterometer for field measurements of sea ice. *IEEE Trans. Geosci. Remote Sens.*, **45**(11), 3405–3416 (doi: 10.1109/TGRS.2007.907043)
- Hallikainen MT, Ulaby FT and Abdelrazik M (1986) Dielectric properties of snow in the 3 to 37 GHz range. *IEEE Trans. Antennas Propag.*, **34**(11), 1329–1340 (doi: 10.1109/TAP.1986.1143757)
- Jonas T, Marty C and Magnusson J (2009) Estimating the snow water equivalent from snow depth measurements in the Swiss Alps. *J. Hydrol.*, **378**(1–2), 161–167 (doi: 10.1016/j.jhydrol.2009.09.021)
- Kershaw GP and McCulloch J (2007) Midwinter snowpack variation across the Arctic treeline, Churchill, Manitoba, Canada. *Arct. Antarct. Alp. Res.*, **39**(1), 9–15 (doi: 10.1657/1523-0430(2007)39[9:MSVATA]2.0.CO;2)
- King JML, Kelly R, Kasurak A, Duguay C, Gunn G and Mead JB (2013) UW-Scat: a ground-based dual-frequency scatterometer for observation of snow properties. *IEEE Geosci. Remote Sens. Lett.*, **10**(3), 528–532 (doi: 10.1109/LGRS.2012.2212177)
- Marshall H-P and Koh G (2008) FMCW radars for snow research. *Cold Reg. Sci. Technol.*, **52**(2), 118–131 (doi: 10.1016/j.coldregions.2007.04.008)
- Marshall HP, Koh G and Forster RR (2004) Ground-based frequency-modulated continuous wave radar measurements in wet and dry snowpacks, Colorado, USA: an analysis and summary of the 2002–03 NASA CLPX data. *Hydrol. Process.*, **18**(18), 3609–3622 (doi: 10.1002/hyp.5804)
- Marshall H-P, Schneebeli M and Koh G (2007) Snow stratigraphy measurements with high-frequency FMCW radar: comparison with snow micro-penetrator. *Cold Reg. Sci. Technol.*, **47**(1–2), 108–117 (doi: 10.1016/j.coldregions.2006.08.008)
- Mätzler C (1987) Applications of the interaction of microwaves with the natural snow cover. *Remote Sens. Rev.*, **2**(2), 259–387 (doi: 10.1080/02757258709532086)
- Montpetit B, Royer A, Roy A, Langlois A and Derksen C (2013) Snow microwave emission modeling of ice lenses within a snowpack using the microwave emission model for layered snowpacks. *IEEE Trans. Geosci. Remote Sens.*, **51**(9), 4705–4717 (doi: 10.1109/TGRS.2013.2250509)
- Morrison K and Bennett J (2014) Tomographic profiling: a technique for multi-incidence-angle retrieval of the vertical SAR backscattering profiles of biogeophysical targets. *IEEE Trans. Geosci. Remote Sens.*, **52**(2), 1350–1355 (doi: 10.1109/TGRS.2013.2250508)
- Pomeroy JW, Marsh P and Gray DM (1997) Application of a distributed blowing snow model to the Arctic. *Hydrol. Process.*, **11**(11), 1451–1464 (doi: 10.1002/(SICI)1099-1085(199709)11:11<1451::AID-HYP449>3.0.CO;2-Q)
- Rees A, English M, Derksen C, Toose P and Silis A (2014) Observations of late winter Canadian tundra snow cover properties. *Hydrol. Process.*, **28**(12), 3962–3977 (doi: 10.1002/hyp.9931)
- Rott H and 13 others (2010) Cold Regions Hydrology High-resolution Observatory for snow and cold land processes. *Proc. IEEE*, **98**(5), 752–765 (doi: 10.1109/JPROC.2009.2038947)
- Scipi6n DE, Mott R, Lehning M, Schneebeli M and Berne A (2013) Seasonal small-scale spatial variability in alpine snowfall and snow accumulation. *Water Resour. Res.*, **49**(3), 1446–1457 (doi: 10.1002/wrcr.20135)
- Sturm M and Benson CS (1997) Vapor transport, grain growth and depth-hoar development in the subarctic snow. *J. Glaciol.*, **43**(143), 42–59

- Sturm M and Benson C (2004) Scales of spatial heterogeneity for perennial and seasonal snow layers. *Ann. Glaciol.*, **38**, 253–260 (doi: 10.3189/172756404781815112)
- Sturm M and Wagner AM (2010) Using repeated patterns in snow distribution modeling: an Arctic example. *Water Resour. Res.*, **46**(W12), W12549 (doi: 10.1029/2010WR009434)
- Sturm M, Holmgren J and Liston GE (1995) A seasonal snow cover classification scheme for local to global applications. *J. Climate*, **8**(5), 1261–1283
- Tape KD, Rutter N, Marshall, HP, Essery R and Sturm M (2010) Recording microscale variations in snowpack layering using near-infrared photography. *J. Glaciol.*, **56**(195), 75–80 (doi: 10.3189/002214310791190938)
- Tsang L, Pan J, Liang D, Li Z, Cline DW and Tan T (2007) Modeling active microwave remote sensing of snow using dense media radiative transfer (DMRT) theory with multiple-scattering effects. *IEEE Trans. Geosci. Remote Sens.*, **45**(4), 990–1004 (doi: 10.1109/TGRS.2006.888854)
- Ulaby FT, Moore RK and Fung AK (1982) *Microwave remote sensing, active and passive. Vol. II. Radar remote sensing and surface scattering and emission theory.* Artech House, Norwood, MA
- Willatt RC, Giles KA, Laxon SW, Stone-Drake L and Worby AP (2010) Field investigations of Ku-Band radar penetration into snow cover on Antarctic sea ice. *IEEE Trans. Geosci. Remote Sens.*, **48**(1), 365–372 (doi: 10.1109/TGRS.2009.2028237)
- Yueh S, Dinardo SJ, Akgiray A, West R, Cline DW and Elder K (2009) Airborne Ku-band polarimetric radar remote sensing of terrestrial snow cover. *IEEE Trans. Geosci. Remote Sens.*, **47**(10), 3347–3364 (doi: 10.1109/TGRS.2009.2022945)

MS received 23 January 2014 and accepted in revised form 12 October 2014